Construction of a cuproptosis-related lncRNA signature to predict biochemical recurrence of prostate cancer

ZHAOJUN YU, HUANHUAN DENG, HAICHAO CHAO, ZHEN SONG and TAO ZENG

Urology Department, The Second Affiliated Hospital of Nanchang University, Nanchang, Jiangxi 330006, P.R. China

Received September 3, 2023; Accepted April 29, 2024

DOI: 10.3892/ol.2024.14659

Abstract. Biochemical recurrence (BCR) is common in prostate cancer (PCa), and patients with BCR usually have a poor prognosis. Cuproptosis is a unique type of cell death, and copper homeostasis is crucial to the occurrence and development of malignancies. The present study aimed to explore the prognostic value of cuproptosis-related long non-coding RNAs (lncRNAs; CRLs) in PCa and to develop a predictive signature for forecasting BCR in patients with PCa. Using The Cancer Genome Atlas database, transcriptomic, mutation and clinical data were collected from patients with PCa. A total of 121 CRLs were identified using Pearson's correlation coefficient. Subsequently, a 6-CRL signature consisting of AC087276.2, CNNM3-DT, AC090198.1, AC138207.5, METTL14-DT and LINC01515 was created to predict the BCR of patients with PCa through Cox and least absolute shrinkage and selection operator regression analyses. Kaplan-Meier curve analysis demonstrated that high-risk patients had a low BCR-free survival rate. In addition, there was a substantial difference between the high- and low-risk groups in the immune microenvironment, immune therapy, drug sensitivity and tumor mutational burden. A nomogram integrating the Gleason score, 6-CRL signature and clinical T-stage was established and evaluated. Finally, the expression of signature lncRNAs in PCa cells was verified through reverse transcription-quantitative PCR. In conclusion, the 6-CRL signature may be a potential tool for making predictions regarding BCR in patients with PCa, and the prognostic nomogram may be considered a practical tool for clinical decision-making.

Correspondence to: Dr Tao Zeng, Urology Department, The Second Affiliated Hospital of Nanchang University, 1 Minde Road, Donghu, Nanchang, Jiangxi 330006, P.R. China
E-mail: lcau002@126.com

Abbreviations: AUC, area under the ROC; C-index, conformance index; CRGs, cuproptosis-related genes; CRLs, cuproptosis-related lncRNAs; GO, Gene Ontology; IC_{50}, half maximal inhibitory concentration; KEGG, Kyoto Encyclopedia of Genes and Genomes; K-M, Kaplan-Meier; LASSO, least absolute shrinkage and selection operator; lncRNA, long noncoding RNA; PCa, prostate cancer; PFS, progression-free survival; ROC, receiver operating curve; TIDE, tumor immune dysfunction and exclusion; TMB, tumor mutation burden

Key words: PCa, signature, prognosis, biochemical recurrence

Introduction

Prostate cancer (PCa) is one of the most common malignant tumors in men (1). In 2021, ~248,530 new PCa cases were diagnosed and ~34,130 male patients died from PCa in the United States, according to the National Cancer Institute (2). Surgical resection can only effectively treat PCa at the early stages (3); however, in most cases, patients are not suiTable for surgical treatment due to being diagnosed at an advanced stage. The treatment options for the middle and advanced stages of PCa include chemotherapy, endocrine therapy and radiotherapy (4). Despite these treatments being performed in the early stages, numerous patients face the risk of resistance to treatment and biochemical recurrence (BCR) (4). BCR occurs in 15-45% of treated patients (5), and it affects both patient survival and quality of life. Early identification of the patients at a high risk of BCR serves an essential role in improving patient prognosis.

Copper, an essential trace element with oxidative and essential biological properties, is the third most abundant transition metal ion (6). Copper is a critical cofactor in a number of metalloproteins; hence, a comprehensive biological system for balancing copper concentration is essential. Copper deficiency or excess are known causes of Wilson and Menkes diseases, respectively, and copper concentration in cancer cells is higher than that in normal cells (7,8). Cuproptosis, a unique mode of cell death resulting from copper accumulation in cells, was recently introduced by the Harvard-MIT Broad Institute (9). This form of cell death differs from the currently known signaling cascades and molecularly defined effector mechanisms of cell death, such as necroptosis, pyroptosis and apoptosis (10). Copper binds to DLAT, resulting in its oligomerization and reduced lipid acylation leading to reduced Fe-S cluster proteins, glutathione depletion and decreased mitochondrial respiration levels (9). In contrast to the Warburg effect, cancerous prostate tissue increases mitochondrial energy metabolism (11). Exploring copper-related genes may provide a strategy for identifying novel biomarkers for PCa prognosis and treatment.

Long non-coding RNA (lncRNA) is a non-coding RNA molecule that consists of >200 nucleotides (12). In addition to transcriptional, silencing, chromosome modification and

intranuclear transport functions, lncRNAs can reprogram the energy metabolism of cancer cells (13). Previous studies have suggested that lncRNAs may function as biomarkers for several malignancies, including hepatocellular carcinoma, lung cancer and PCa (14-16). lncRNAs serve a critical role in PCa proliferation (17), docetaxel and enzalutamide resistance (18,19), bone metastasis (20) and energy metabolism (21). Shang *et al* (22) reported that the lncRNA PCAT1 can activate the AKT and NF-κB signaling pathways in castration-resistant PCa.

For PCa, BCR risk prediction is mainly based on clinicopathological parameters, including prostate-specific antigen (PSA), Gleason score, tumor pathology and T stage (23,24). The classification of the BCR risk population based on the Gleason score and PSA doubling time, as recommended by the European Association of Urology guidelines, is not highly accurate for predicting the clinical outcome of patients (25). Therefore, the existing strategies for assessing the risk of BCR in patients with PCa based on clinicopathological parameters need to be further optimized. Inappropriate risk assessment may lead to overtreatment, a waste of medical resources and can increase the economic burden of patients. Due to the rapid development of sequencing technology, biomarker identification based on DNA, RNA or protein is becoming increasingly important in the diagnosis, treatment and prognosis of diseases (26,27). Notably, cuproptosis is closely related to cancer development, and an increasing number of studies have shown that lncRNA can be used as an essential marker of diagnosis, prognosis and treatment in tumors (15,28,29); therefore, the construction of a signature based on cuproptosis-related lncRNAs (CRLs) to predict the prognosis of patients with PCa, especially BCR, was investigated. The aim of the present study was to construct a CRL signature for predicting the BCR of patients with PCa, and to explore the predictive accuracy of this signature.

Materials and methods

Data collection. Using The Cancer Genome Atlas Prostate Adenocarcinoma (TCGA-PRAD) dataset, the transcriptomic (Tpm) and gene mutation data (originating from the 'simple nucleotide variation' file), and the clinical information of 497 patients with PCa were extracted (https://portal.gdc.cancer.gov). Next, those patients with PCa who satisfied the following criteria were included in the present study: i) Patients with clear BCR data, including the BCR status and time; and ii) patients with complete and clear follow-up data. To minimize information and statistical biases, the following exclusion criteria were applied: i) Patient follow up time was <30 days; and ii) patients without clear BCR and follow-up data. Finally, 418 patients with PCa were included in the current study. A total of 19 cuproptosis-related genes (CRGs) were obtained from published research (30-35).

Construction of the CRL signature. lncRNAs associated with cuproptosis were identified using Pearson's correlation coefficient, with cut-off criteria of P<0.001 and |R|>0.3. A Sankey diagram was drawn through R package 'ggalluvial' (http://corybrunson.github.io/ggalluvial/) and 'ggplot2' (https://ggplot2.tidyverse.org) to show the correlation between lncRNA and CRGs. For the purpose of constructing and validating a predictive signature correlated with the BCR-free survival (BFS) of patients with PCa, a ratio of 7:3 was applied to divide the 418 samples into training and testing sets [training set (n=295) and testing set (n=123)]. All samples were identified as the entire set. The clinicopathological data of the three sets (training set, testing set and entire set) are described in Table I. To identify the association of CRLs with the BFS of patients with PCa, univariate Cox regression analysis was used. Those lncRNAs with P<0.05 were subjected to least absolute shrinkage and selection operator (LASSO) regression analysis. Subsequently, the R package 'glmnet' (https://glmnet.stanford.edu) was used to lower the risk of overfitting with LASSO regression. To select the final candidates and construct the signature, a stepwise multivariate Cox regression analysis was used. lncRNAs with P<0.05 were identified as the final genes. The validation was performed on both the testing and the entire sets. Using the following formula, the risk of every patient with PCa was computed. The formula was as follows: Risk score=(LINC01515x1.4055761678005+AC090198.1x0.171855258101095+AC087276.2x-1.75799460466145+AC138207.5x0.130718896321139+CNNM3-DTx0.0800687027705137+METTL14-DTx3.13564874470709).

Validation of the 6-CRL signature in testing and entire sets. Depending on their median risk scores, the patients were categorized into high- and low-risk groups. Kaplan-Meier (K-M) survival curves were analyzed using the R package 'survival' (https://github.com/therneau/survival) to estimate differences in BFS between the two groups. The R packages 'Rtsne' (https://lvdmaaten.github.io/tsne/), 'timeROC' (https://CRAN.R-project.org/package=timeROC) and 'survival' were used to conduct principal component analysis and time-dependent receiver operating characteristic (ROC) curve analysis, to assess the stability and accuracy of the signature. Additionally, the R packages 'rms' (https://hbiostat.org/R/rms/), and 'pec' (https://CRAN.R-project.org/package=pec) were used to conduct conformance index (C-index) analysis.

Independent prognostic analysis. To identify the independent prognostic indicators associated with the BFS of patients with PCa, univariate and multivariate Cox regression analyses were carried out.

Subset group K-M survival analysis for BFS. A stratified analysis was conducted to examine if the signature maintained predictive capacity across subgroups (age, and pathological and clinical T-stage) using the 'survival' R package.

Construction and evaluation of a nomogram. A nomogram was developed to predict 1-, 3- and 5-year BFS using the R software 'regplot' package (https://CRAN.R-project.org/package=regplot). The prognostic accuracy was evaluated using the ROC and calibration curve analyses.

Functional enrichment analysis and immune analysis. The 'limma' R package (https://bioinf.wehi.edu.au/limma/) was used to conduct a differential expression analysis between high- and low-risk samples (criteria: |log2 fold change|>1 and P<0.05). The 'Clusterfiler' R package (https://yulab-smu.

Table I. Clinicopathological characteristics of selected patients with prostate cancer in the training set, testing set and entire set.

Clinical characteristic	Training set (%)	Testing set (%)	Entire set (%)	P-value
Age, years				0.562
≤65	210 (71.19)	91 (73.98)	301 (72.01)	
>65	85 (28.81)	32 (26.02)	117 (27.99)	
cT stage				0.159
T1	102 (34.58)	48 (39.02)	150 (35.89)	
T2	105 (35.59)	47 (38.21)	152 (36.36)	
T3	39 (13.22)	8 (6.50)	47 (11.24)	
T4	0 (0.00)	1 (0.81)	1 (0.24)	
Unknown	49 (16.61)	19 (15.45)	68 (16.27)	
pN stage				0.876
N0	209 (70.85)	89 (72.36)	298 (71.29)	
N1	47 (15.93)	20 (16.26)	67 (16.03)	
Unknown	39 (13.22)	14 (11.38)	53 (12.68)	
pT stage				0.073
T2	96 (32.54)	55 (44.72)	151 (36.12)	
T3	191 (64.75)	64 (52.03)	255 (61.00)	
T4	5 (1.69)	2 (1.63)	7 (1.67)	
Unknown	3 (1.02)	2 (1.63)	5 (1.20)	
Gleason score				0.634
6	28 (9.49)	9 (7.32)	37 (8.85)	
7	139 (47.12)	64 (52.03)	203 (48.56)	
8	38 (12.88)	19 (15.45)	57 (13.64)	
9	87 (29.49)	31 (25.2)	118 (28.23)	
10	3 (1.02)	0 (0)	3 (0.72)	

top/biomedical-knowledge-mining-book) was used to perform Gene Ontology (GO) and Kyoto Encyclopedia of Genes and Genomes (KEGG) enrichment analyses with the significance threshold set at P<0.05. The R packages 'GOplot' (https://github.com/wencke/wencke.github.io) and 'ggplot2' (https://github.com/tidyverse/ggplot2) were used to present the enrichment analysis results.

In order to evaluate the difference of immune cell infiltration between high- and low-risk PCa samples, the CIBERSORT algorithm was applied to analyze the infiltration of 22 types of immune cells in PCa samples (36). By reviewing the literature, it was revealed that researchers analyzed these 22 types of immune cells; therefore, these 22 immune cells were selected for the present study (37-39). The 'ggpubr' package (https://rpkgs.datanovia.com/ggpubr/) was used to draw boxplots. To evaluate the reactivity of immunotherapy in different risk groups, the tumor immune dysfunction and exclusion (TIDE) score files of PCa were obtained from the TIDE website (http://tide.dfci.harvard.edu/) (40), showing the difference in TIDE score between high- and low-risk groups.

Tumor mutational burden (TMB) analysis. The 'maftools' package (https://bioconductor.org/packages/release/bioc/vignettes/maftools/inst/doc/maftools.html) was used to determine the mutation frequency within patients with PCa in different risk groups. The differential analysis of TMB between the high- and low-risk group was conducted to determine whether TMB was related to risk scores. Based on the K-M method, the BFS rates of patients were compared between the low- and high-TMB groups.

Drug sensitivity analysis. To calculate the half maximal inhibitory concentration (IC_{50}) for different drugs, the R packages 'pRophetic' (http://genemed.uchicago.edu/~pgeeleher/pRRophetic/) and 'ggplot2' were used. The Wilcoxon rank sum test was applied to compare the IC_{50} values between the high- and low-risk groups.

Cell culture and reverse transcription-quantitative PCR (RT-qPCR). The immortalized prostate primary epithelial cell line RWPE1, and the PCa cell lines PC3 and DU145 were obtained from the American Type Culture Collection. According to the manufacturer's instructions, RWPE1 cells were grown in serum-free keratinocyte medium (ScienCell Research Laboratories, Inc.), PC3 cells were cultured in F12K medium and DU145 cells were cultured in the RPMI 1640 medium (Gibco; Thermo Fisher Scientific, Inc.). The aforementioned media were supplemented with 1% penicillin/streptomycin and 10% FBS (Shanghai ExCell Biology, Inc.). Cells were cultured at 37˚C and 5% CO_2.

TRIzol® (Invitrogen; Thermo Fisher Scientific, Inc.) was used for RNA extraction. In accordance with the manufacturer's

Table II. Primer sequences of signature long noncoding RNAs and ACTB.

Primer	Forward sequence, 5'-3'	Reverse sequence, 5'-3'
LINC01515	GTCCGAAGCAAGACATGTGAC	GCTAAACTGCCCAGTGGCAT
CNNM3-DT	TCAGCACACTCAATCGCACA	TTCGTCCACACCTACAGGCT
METTL14-DT	AATCATGGACGATGCTGCCA	GGAAAGTGAGGTGCTCTCCA
AC090198.1	CAGCAGCCACAGTTGGAAATC	TCTCTCGCAAGGGTAGAGGT
AC087276.2	ACCCTCCAATCTGTATCACTGG	TCCTTGGCAAAGGTGGTAGC
AC138207.5	TGAGACAGGGTCTTTGTTGC	AAATTTCAGGGCTGGACGTG
ACTB	TCTCCCAAGTCCACACAGG	GGCACGAAGGCTCATCA

instructions, a RT kit (Tiangen Biotech Co., Ltd.) was used for RT, according to the manufacturer's protocol. Subsequently, fluorescence qPCR was conducted according to the manufacturer's instructions using StepOne Plus (Applied Biosystems; Thermo Fisher Scientific, Inc.) and SYBR Green qPCR Mix (Thermo Fisher Scientific, Inc.). The primers used for qPCR were obtained from Sangon Biotech Co., Ltd., and the sequences are shown in Table II. The thermocycling conditions used for qPCR were: 30 sec at 95˚C for 1 cycle; followed by 40 cycles at 95˚C for 15 sec and 60˚C for 30 sec. ACTB was used as an internal control for normalization, and the $2^{-\Delta\Delta Cq}$ method was used to calculate the relative mRNA expression (41).

Statistical analysis. R software (version 4.2.0; https://www.r-project.org/) was used to conduct the bioinformatics analysis. qPCR data were analyzed using GraphPad Prism (version 9.5; Dotmatics) by one-way ANOVA and Dunnett's multiple comparisons post hoc test. The χ^2 test or Fisher's exact test was used to statistically analyze the clinicopathological characteristics between the training and testing sets. Survival differences between high- and low-risk groups were assessed using log-rank test. Statistical differences in quantitative data between high- and low-risk groups were determined by unpaired Student's t-test. Unless otherwise indicated, $P<0.05$ was considered to indicate a statistically significant difference.

Results

Identification of CRLs. The overall flowchart of the present study is shown in Fig. 1. Based on the exclusion criteria, 418 PCa samples were obtained from TCGA database, along with Tpm and clinical data. The clinical parameters of the selected patients are given in detail in Table I. The statistical analysis showed no significant difference between the training and testing sets regarding clinicopathological features, including age, clinical T stage, pathological N stage, pathological T stage and Gleason score. A total of 19 CRGs were obtained from previous studies (30-35), and the related gene expression profile was extracted from TCGA-PRAD dataset. A total of 121 lncRNAs were identified as CRLs by investigating the association between lncRNAs and CRGs. Moreover, the internal connections between CRLs and CRGs were visualized using a Sankey diagram (Fig. S1).

Establishment of the CRL prognostic signature. To determine the CRLs associated with the BFS of patients with PCa, a univariate Cox regression analysis was conducted, and 18 CRLs were obtained (Fig. 2A). Subsequently, these CRLs were subjected to LASSO regression analysis (Fig. 2B and C). Finally, six CRLs were identified and used to build a prognostic signature using step-wise multivariate Cox regression (Table III). In TCGA-PRAD dataset, all patients had calculated risk scores according to the aforementioned signature.

Depending on the median risk score, patients were categorized into high- and low-risk groups. The distribution of risk scores for patients with PCa is shown in Fig. 2D. Notably, as the risk score increased, the BCR rate increased (Fig. 2F). A total of 5/6 signature lncRNAs (LINC01515, AC090198.1, AC138207.5, CNNM3-DT and METTL14-DT) exhibited increased expression in the high-risk group compared with in the low-risk group, whereas AC087276.2 had lower expression (Fig. 2E). The K-M survival analysis revealed that patients at high risk had a worse BFS rate ($P=8.03\times10^{-6}$; Fig. 2H). For the 1-, 3- and 5-year BFS of the signature, the area under the ROC curve (AUC) values were 0.728, 0.740 and 0.783, respectively, which suggested that the signature accurately predicted the BFS of patients with PCa (Fig. 2G).

Validation of the CRL signature. The predictive ability of the risk signature was confirmed in the testing and entire sets. In both sets, the risk scores of patients with PCa were determined using the same formula, and the same cut-off value was used to classify patients into high- and low-risk groups. The risk score and BCR status distribution for the two sets are shown in Fig. 3A-D. In addition, the expression of the 6-CRL signature genes in different risk groups in the testing set (Fig. 3E) and entire set (Fig. 3F) was shown through heat maps. Subsequently, the K-M survival analysis revealed a considerable difference in the BFS rate between different risk groups (testing set, $P=2.08\times10^{-2}$ entire set, $P=7.56\times10^{-7}$; Fig. 3G and H).

Moreover, AUCs for the 1-, 3- and 5-year BFS rates for the testing set were 0.667, 0.715 and 0.831, respectively (Fig. 3I), while the relevant values for the entire set were 0.717, 0.729 and 0.781, respectively (Fig. 3J). Principal component analysis was conducted to assess if the 6-CRL signature could identify patients with different risk. It was found that the signature could clearly distinguish between patients with different risks across all sets (Fig. S2A-C). The 6-CRL signature provided excellent performance in both the testing and entire sets. In addition, the relationship between the 6-CRL signature lncRNAs and the 19 CRGs is

Table III. Multivariate Cox stepwise regression analysis of 6 cuproptosis-related long noncoding RNAs associated with biological recurrence-free survival in patients with prostate cancer.

ID	Coefficient	HR	HR.95L	HR.95H	P-value
LINC01515	1.405576	4.077876	1.725672	9.636284	0.001358
AC090198.1	0.171855	1.187506	0.997997	1.413001	0.052701
AC087276.2	-1.75799	0.17239	0.062314	0.476914	0.000709
AC138207.5	0.130719	1.139647	0.976757	1.329702	0.09669
CNNM3-DT	0.080069	1.083361	0.985118	1.191403	0.098774
METTL14-DT	3.135649	23.00355	3.594882	147.1991	0.000929

HR, hazard ratio; HR.95L, high 95% confidence interval of HR; HR.95L, low 95% confidence interval of HR.

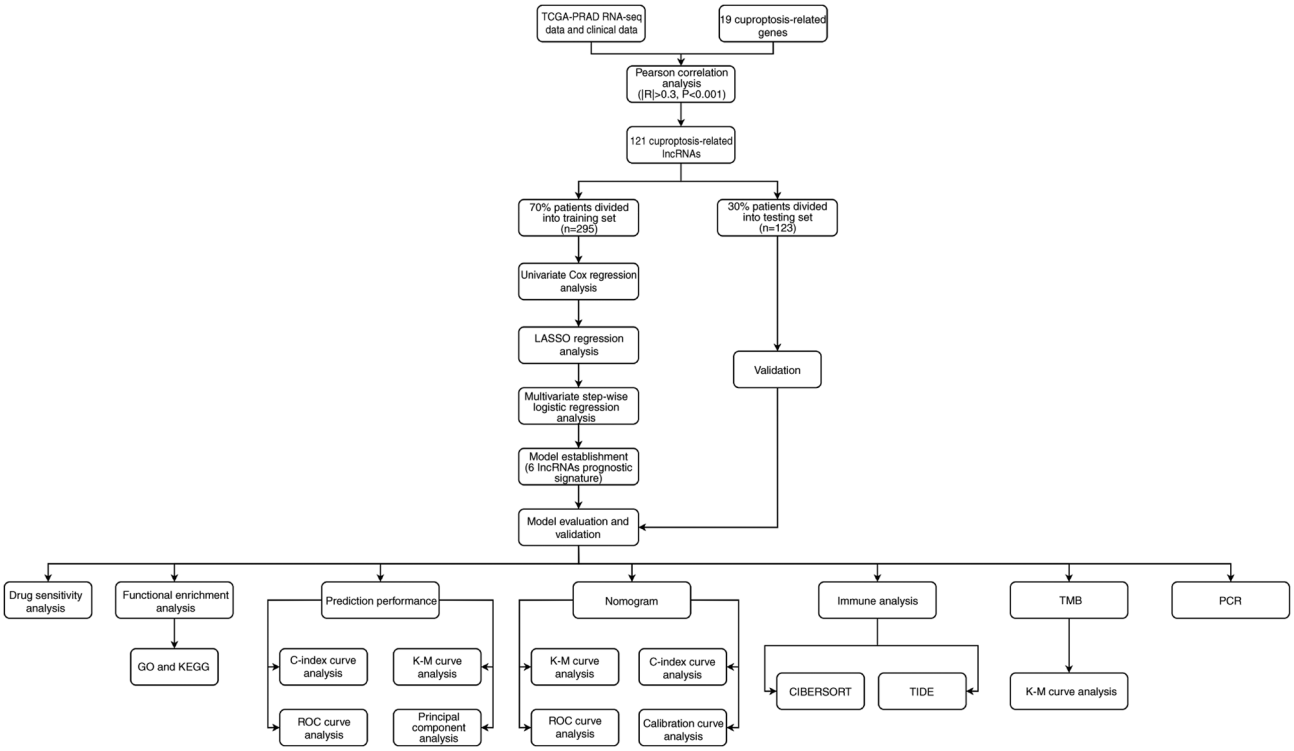

Figure 1. Flowchart of the present study. TCGA-PRAD, The Cancer Genome Atlas Prostate Adenocarcinoma; lncRNA, long noncoding RNA; LASSO, least absolute shrinkage and selection operator; GO, Gene Ontology; KEGG, Kyoto Encyclopedia of Genes and Genomes; K-M, Kaplan-Meier; ROC, receiver operating characteristic; TIDE, tumor immune dysfunction and exclusion.

displayed in Fig. S2D. The results showed that AC087276.2 was closely related with 15 CRGs, AC090198.1 with 17 CRGs, AC138207.5 with five CRGs, CNNM3-DT with seven CRGs, LINC01515 with 13 CRGs, and METTL14-DT with 10 CRGs. The lncRNAs most closely associated with CRGs were AC090198.1, AC087276.2, and LINC0151515. In addition, the association between the 6-CRL signature and progression-free survival (PFS) was investigated using the K-M survival analysis. A lower PFS was found to be associated with high-risk patients in all sets (Fig. S3A-C). The C-index analysis revealed that the C-index values of the signature were 0.737, 0.624 and 0.712 in the training, testing and entire sets, respectively (Table SI). This indicated that the signature's accuracy was highest in the training set, followed by the entire set and testing set.

Independent and subgroup analyses. Cox regression analysis was performed in every dataset. The results showed that the clinical T stage and the 6-CRL signature were the independent variables related to the BFS of patients with PCa in the training set; in the testing set, the clinical T stage and Gleason score were independent factors; in the entire set, the clinical T stage, Gleason score and the 6-CRL signature were independent prognostic factors (Table IV).

Moreover, the applicability of the 6-CRL signature was evaluated by performing a subgroup K-M survival analysis of clinical characteristics, including pathological T stage, clinical T stage and age. A worse BFS was observed for patients at high risk in each subgroup, showing that the signature had good applicability in all patients at early and advanced stages (Fig. S3D-I).

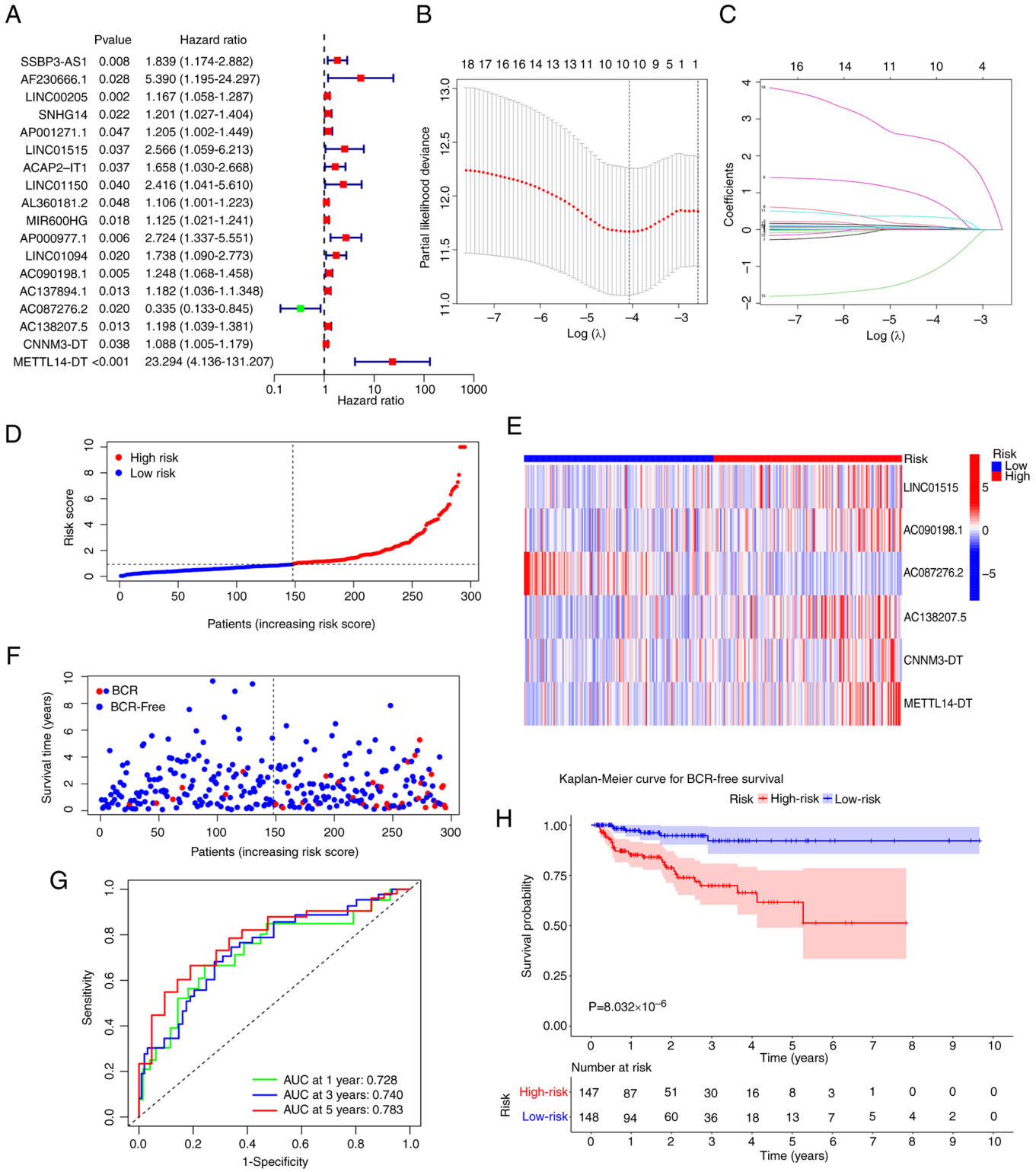

Figure 2. Signature construction based on CRLs in the training set. (A) Forest plot showed the univariate Cox regression analysis of CRLs. (B) In the LASSO analysis, the optimal penalty λ value was chosen. (C) LASSO coefficient profiles of 10 CRLs. (D) Risk score plot showed the distribution of the risk score of each patient with PCa. (E) Heatmap showed the differential expression of six prognostic-related CRLs for each patient. (F) Scatter plot showed the BCR status and BFS time of patients with PCa with different risk scores. (G) Receiver operating characteristic curves for the 6-CRL signature at 1, 3 and 5 years. (H) Survival analysis showed the Kaplan-Meier survival curves of the BCR-free survival between the different risk groups. CRL, cuproptosis-related long noncoding RNA; LASSO, least absolute shrinkage and selection operator; PCa, prostate cancer; BCR, biochemical recurrence; BFS, BCR-free survival; AUC, area under the receiver operating characteristic curve.

Construction and evaluation of a nomogram. To predict the 1-, 3- and 5-year BFS rates for patients with PCa, a nomogram containing risk and Gleason scores, and clinical T stages was developed (Fig. 4A). The K-M analysis implicated that patients with high risk evaluated by the nomogram had a poorer prognosis than those with low risk (Fig. 4B). C-index

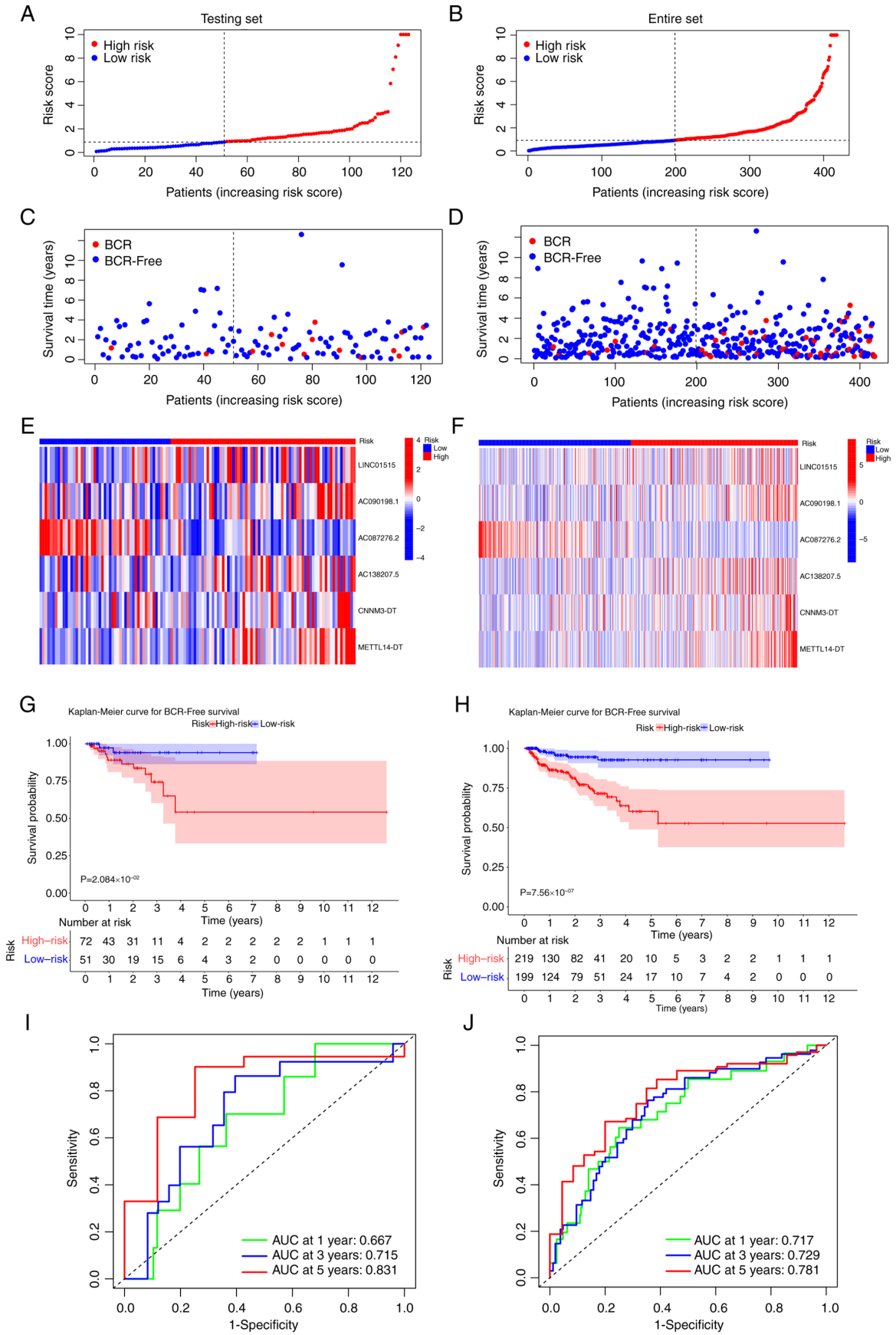

Figure 3. Validation of the 6-CRL prognostic signature in testing and entire sets. Risk score plot showed the distribution of the risk scores for each patient with PCa in the (A) testing set and (B) entire set (B). The scatter plot showed the BCR status and survival time of patients with PCa with different risk scores in the (C) testing set and (D) entire set (D). The heatmap showed the differential expression of the six signature lncRNAs for each patient in the (E) testing set and (F) entire set (F). The survival analysis showed the Kaplan-Meier survival curves of the BCR-free survival between different risk groups in the (G) testing set and (H) entire set (H). Receiver operating characteristic curves for the 6-CRL signature at 1, 3 and 5 years in (I) testing set and (J) entire set. CRL, cuproptosis-related long noncoding RNA; PCa, prostate cancer; BCR, biochemical recurrence; AUC, area under the receiver operating characteristic curve.

Table IV. Cox analysis of the signature and clinicopathological traits in each set.

A, Training set

	Univariate analysis		Multivariate analysis	
Variable	HR (95% CI)	P-value	HR (95% CI)	P-value
Age	1.022 (0.972-1.075)	0.388	1.005 (0.955- 1.059)	0.835
Clinical				
T stage	2.147 (1.337- 3.448)	0.002	1.731 (1.009- 2.970)	0.046
Pathological T stage	2.414 (1.134- 5.139)	0.022	1.400 (0.545-3.595)	0.484
Pathological				
N stage	2.005 (0.953-4.215)	0.067	0.972 (0.415-2.277)	0.949
Gleason score	1.547 (1.089- 2.198)	0.014	1.243 (0.815-1.895)	0.313
Risk score	1.112 (1.070- 1.155)	$4.349x10^{-8}$	1.106 (1.063-1.152)	$8.014x10^{-7}$

B, Testing set

	Univariate analysis		Multivariate analysis	
Variable	HR (95% CI)	P-value	HR (95% CI)	P-value
Age	0.993 (0.901-1.094)	0.885	0.942 (0.843-1.053)	0.296
Clinical				
T stage	3.241 (1.329-7.905)	0.010	10.017 (2.295-43.718)	0.002
Pathological T stage	4.871 (1.565-15.156)	0.006	1.327 (0.172-10.256)	0.786
Pathological				
N stage	3.002 (0.875-10.297)	0.080	0.672 (0.126-3.580)	0.642
Gleason score	3.490 (1.587-7.673)	0.002	6.274 (1.789-22.007)	0.004
Risk score	1.090 (0.953-1.247)	0.207	1.057 (0.875-1.276)	0.566

C, Entire set

	Univariate analysis		Multivariate analysis	
Variable	HR (95% CI)	P-value	HR (95% CI)	P-value
Age	1.016 (0.972-1.062)	0.478	0.995 (0.953-1.040)	0.832
Clinical				
T stage	2.361 (1.555-3.586)	5.546e-05	1.836 (1.177-2.862)	0.007
Pathological T stage	2.931 (1.584-5.422)	0.0006	1.594 (0.725-3.504)	0.246
Pathological				
N stage	2.219 (1.175-4.187)	0.014	0.956 (0.469-1.947)	0.901
Gleason score	1.844 (1.349-2.521)	0.0001	1.480 (1.027-2.134)	0.035
Risk score	1.111 (1.074-1.150)	$1.308x10^{-9}$	1.104 (1.064-1.146)	$1.381x10^{-7}$

and time-dependent ROC curve analysis were applied to assess the prediction accuracy of the nomogram. The findings demonstrated that the 1-, 3- and 5-year AUC values were all >0.75 (Fig. 4C), and the C-index value was 0.744 (range, 0.700-0.788), demonstrating that the predictive performance of the nomogram was strong. Additionally, agreement between the actual and expected BFS rates was found in the calibration plots (Fig. 4D-F), which further confirmed the aforementioned conclusion.

Function and pathway analyses. There were 214 differentially expressed genes (DEGs) identified between the high- and low-risk groups, including 112 upregulated and 102 downregulated genes (Fig. 5A). The mechanism underlying the DEGs was examined using GO and KEGG analyses. The KEGG analysis demonstrated that DEGs were primarily abundant in metabolic pathways and cardiovascular pathways; the metabolic pathways included 'Glycerolipid metabolism' and 'Nitrogen metabolism', and

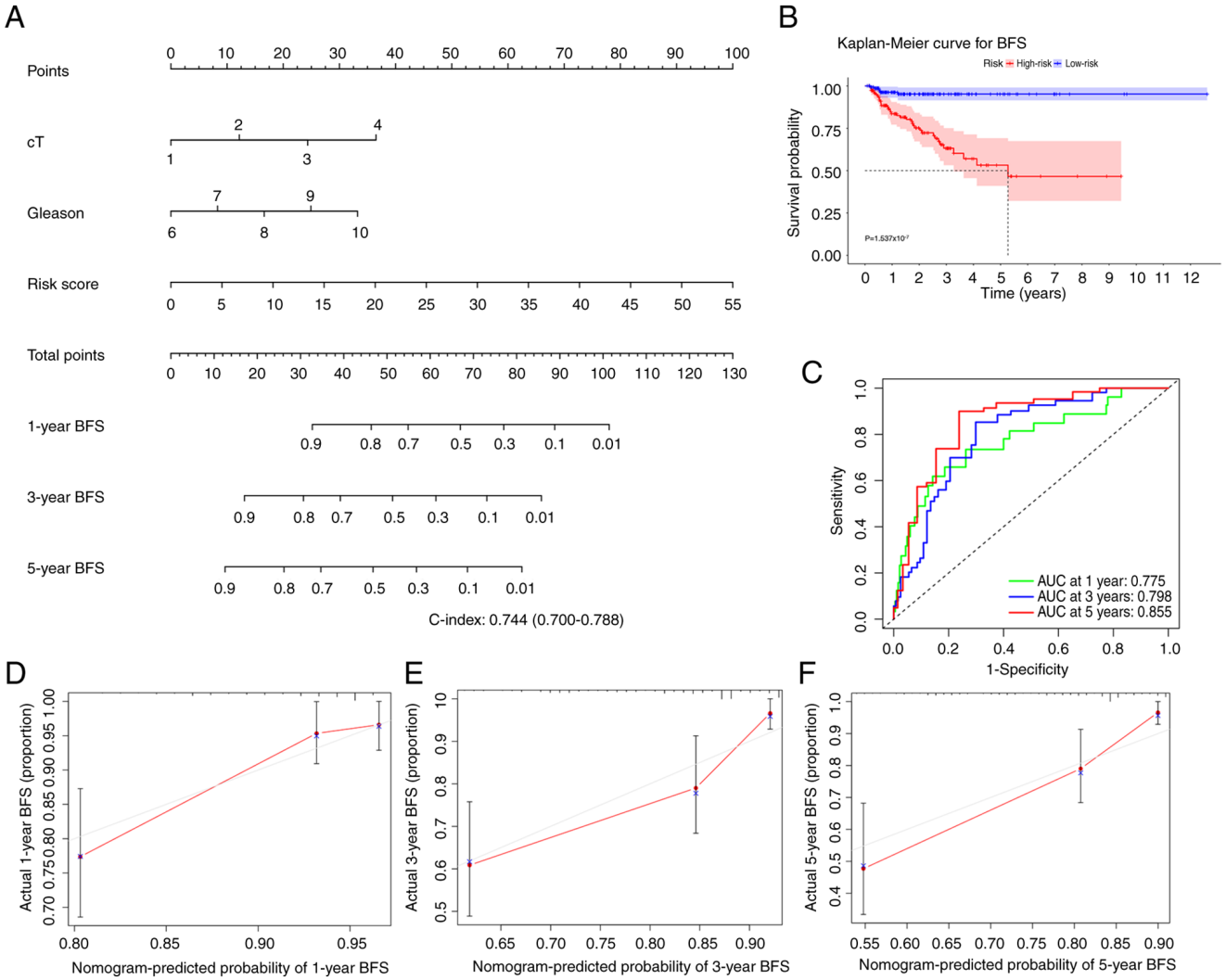

Figure 4. Construction and evaluation of a nomogram. (A) Nomogram showed that the 1-, 3- and 5-year BFS rate of patients with prostate cancer was predicted through the clinical characteristics and risk score. (B) Kaplan-Meier survival curves of the BFS between different nomogram risk groups. (C) Receiver operating characteristic curves for the nomogram at 1-, 3- and 5-years. (D) Calibration curve of the nomogram for forecasting the 1-year BFS rate. (E) Calibration curve of the nomogram for forecasting the 3-year BFS rate. (F) Calibration curve of the nomogram for forecasting the 5-year BFS rate. BFS, biochemical recurrence-free survival; AUC, area under the receiver operating characteristic curve.

the cardiovascular pathways included 'Cardiac muscle contraction', 'Adrenergic signaling in cardiomyocytes', 'Hypertrophic cardiomyopathy', and 'Dilated cardiomyopathy' (Fig. 5B). The GO enrichment analysis indicated that 'muscle system process', 'muscle contraction', and 'striated muscle tissue development' were the main enriched biological process terms. The main enriched cellular component terms were 'contractile fiber', 'myofibril' and 'sarcomere'. The top three enriched molecular function terms were 'structural constituent of muscle', 'actin filament binding' and 'actin binding' (Fig. 5C).

Immune analysis of the 6-CRL signature. The immune cell infiltration in the high- and low-risk groups is presented in Fig. 5D; there was statistically significant difference between the groups regarding immune cells, including M1 macrophages, resting natural killer cells, follicular T helper cells and monocytes. Subsequently, the potential difference in the expression of immune checkpoint genes between the risk groups was investigated. Only IDO1 was downregulated in the high-risk group (Fig. S4A). Immunotherapy response was predicted using the TIDE score. The TIDE score was lower for the high-risk group compared with that of the low-risk group (Fig. 5E), indicating that immunotherapy was more likely to be effective for those at a higher risk. In addition, the present study investigated the difference between dysfunction and exclusion ratings across the risk categories. The results illustrated that the low-risk group had a higher dysfunction score and a lower exclusion score than the high-risk group (Fig. S4B and C).

TMB and drug sensitivity analyses. The characteristics of somatic mutations for the different risk groups are displayed in waterfall plots (Fig. 6A and B). It was revealed that SPOP (15%), TTN (9%) and TP53 (8%) were the three most commonly mutated genes in the high-risk group, meanwhile, the most commonly mutated genes in the low-risk group were TP53 (11%), SPOP (7%) and TTN (11%). However, there were no significant differences in TMB between the low- and high-risk groups (Fig. S4D). As shown

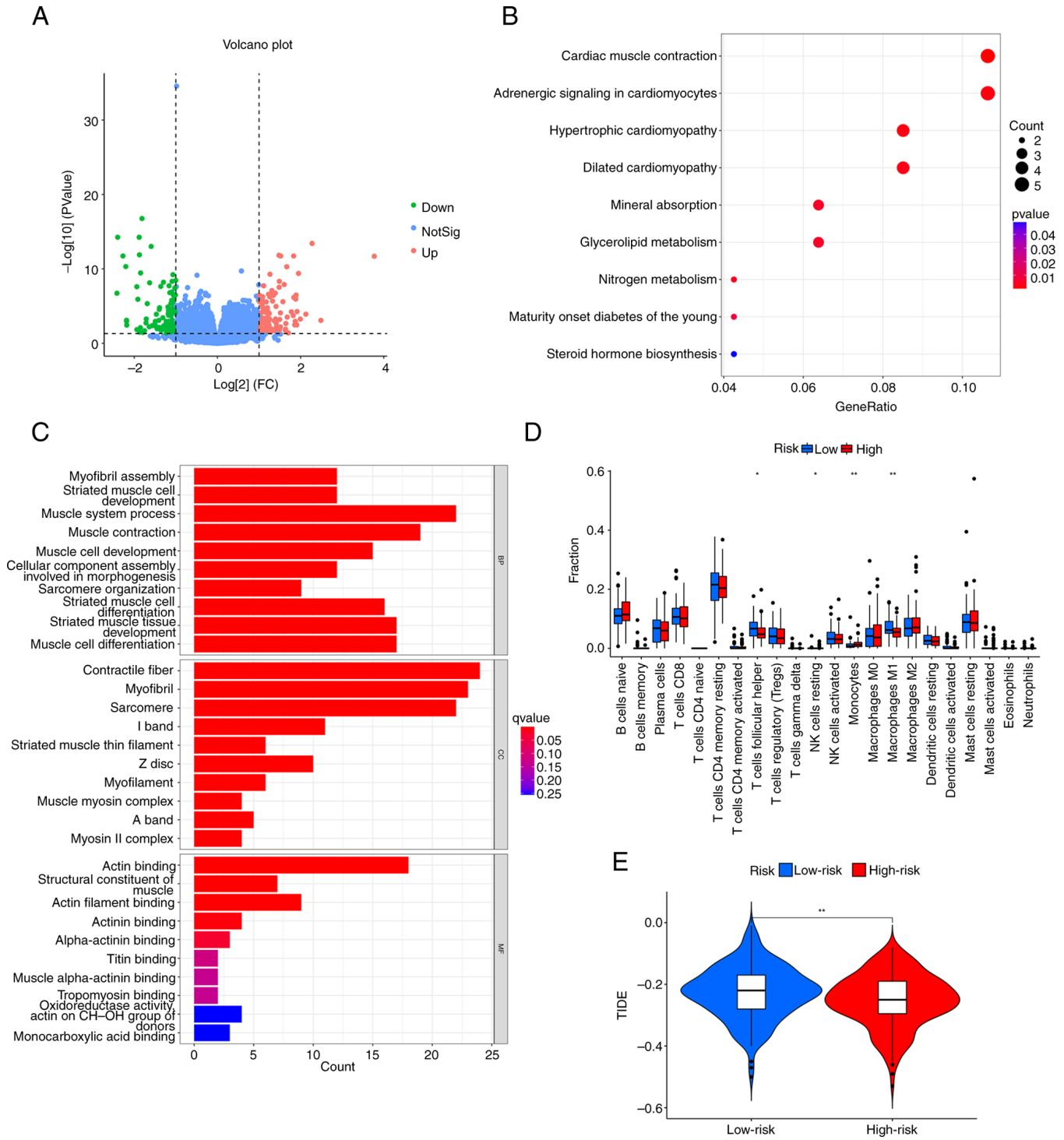

Figure 5. Functional enrichment analysis and immune analysis. (A) Volcano plot for differentially expressed genes between high- and low-risk groups. (B) Kyoto Encyclopedia of Genes and Genomes pathway analysis. (C) Gene Ontology analysis. (D) Immune cell infiltration analysis. (E) TIDE analysis. *P<0.05, **P<0.01. FC, fold change; BP, biological process; CC, cellular component; MF, molecular function; TIDE, tumor immune dysfunction and exclusion.

in Fig. 6C, the K-M survival curves revealed that patients with a higher TMB had a greater likelihood of having a poor BFS. Patients with high TMB but low-risk scores had the greatest BFS rate, whereas those with high TMB and high-risk scores had the lowest BFS rate (Fig. 6D). The present study further examined the variations in drug sensitivity between different risk groups by estimating and comparing the IC_{50} values of the following 10 drugs: Axitinib, bosutinib, bicalutamide, cisplatin, doxorubicin, etoposide, tipifarnib, paclitaxel, sunitinib and gemcitabine. Except for bicalutamide, the IC_{50} values of all medications were lower in the high-risk group (Fig. 7), which indicated that these drugs may be potential anticancer compounds for high-risk patients. Low-risk patients may exhibit a better response to bicalutamide.

Validation of the expression of the signature lncRNAs. Compared with in normal prostate cells, AC087276.2,

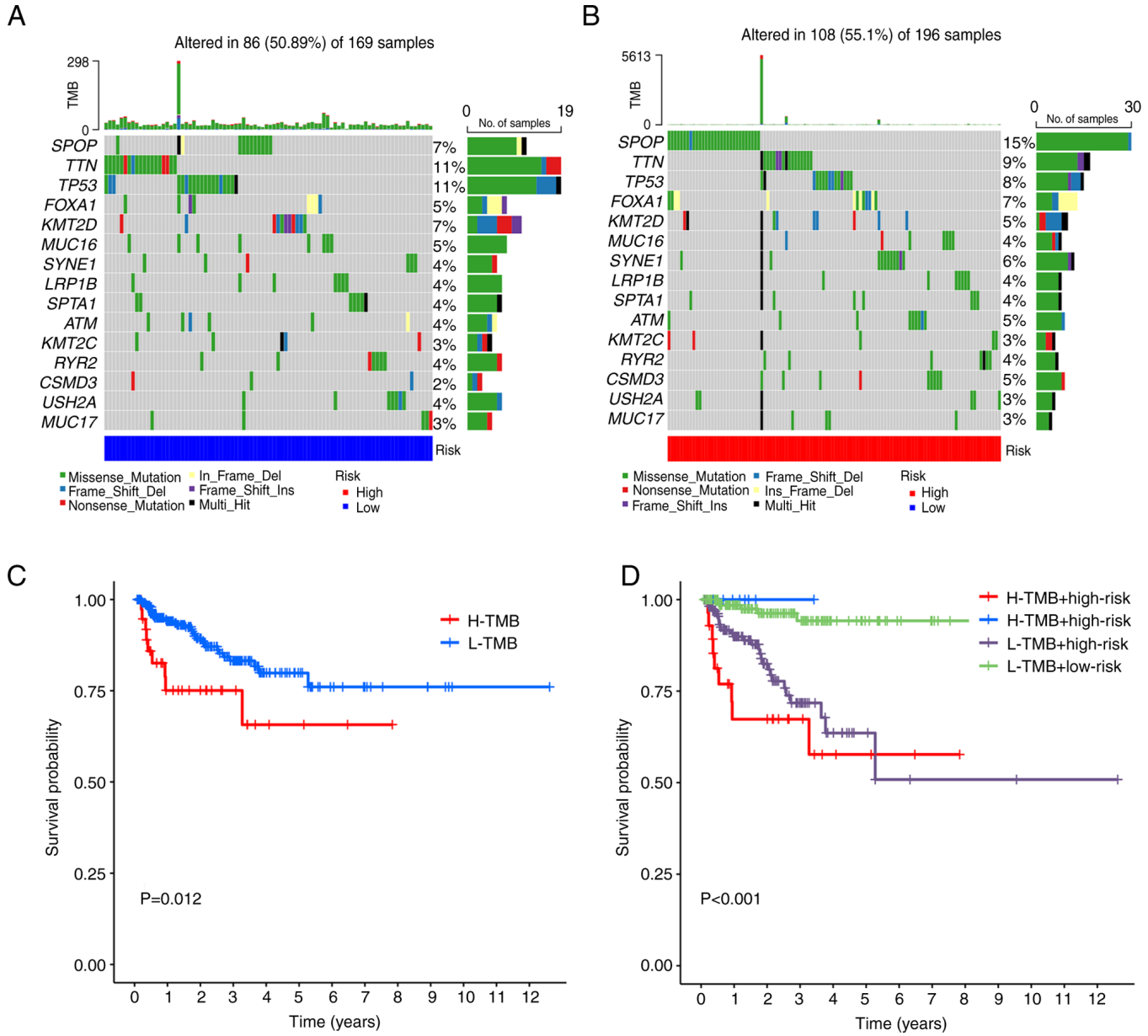

Figure 6. TMB analysis. Top 15 most frequently mutated genes and mutation rate in (A) low-risk and (B) high-risk groups. (C) Kaplan-Meier BCR-free survival analysis of the TMB. (D) Kaplan-Meier BCR-free survival analysis of the TMB and risk score. TMB, tumor mutation burden; BCR, biochemical recurrence.

CNNM3-DT, AC090198.1, AC138207.5 and METTL14-DT were downregulated, whereas LINC01515 was upregulated in PCa cell lines (Fig. 8). Despite the fact that the expression of AC090198.1, AC087276.2 and AC138207.5 was not significantly altered between the RWPE1 cells and DU145 cells, the expression trend was downregulated in the PC3 cells.

Discussion

Patients with PCa and BCR are commonly treated with radiotherapy, chemotherapy and androgen deprivation therapy, increasing the economic burden on patients and reducing their quality of life. In order to improve prognosis, it is crucial to establish biological markers that adequately detect the risk of BCR for patients with PCa. To the best of our knowledge, there is currently no reliable indicator that may predict the risk of BCR for patients with PCa.

Copper homeostasis is crucial for tumor cell growth and proliferation (42,43). Denoyer *et al* (44) reported that the functional supply of copper is essential for the development of PCa in mice. When the copper intake of PCa cells is reduced, the proliferative ability of cells is significantly inhibited (45). Previous studies have shown that the copper signaling pathway may be a promising therapeutic target for PCa (46,47). However, limited research has been carried out on cuproptosis in PCa, and the significance of CRGs in the occurrence and progression of PCa, as well as their prognostic value, remains unclear. In multiple tumors, including hepatocellular carcinoma, glioma and clear cell renal cell carcinoma, the predictive significance of CRLs has been demonstrated (48-50). Despite this, to the best of our knowledge, the prognostic significance of CRLs in PCa has not yet been explored. In addition to establishing a 6-CRL signature for predicting the BFS of patients with PCa, the function of

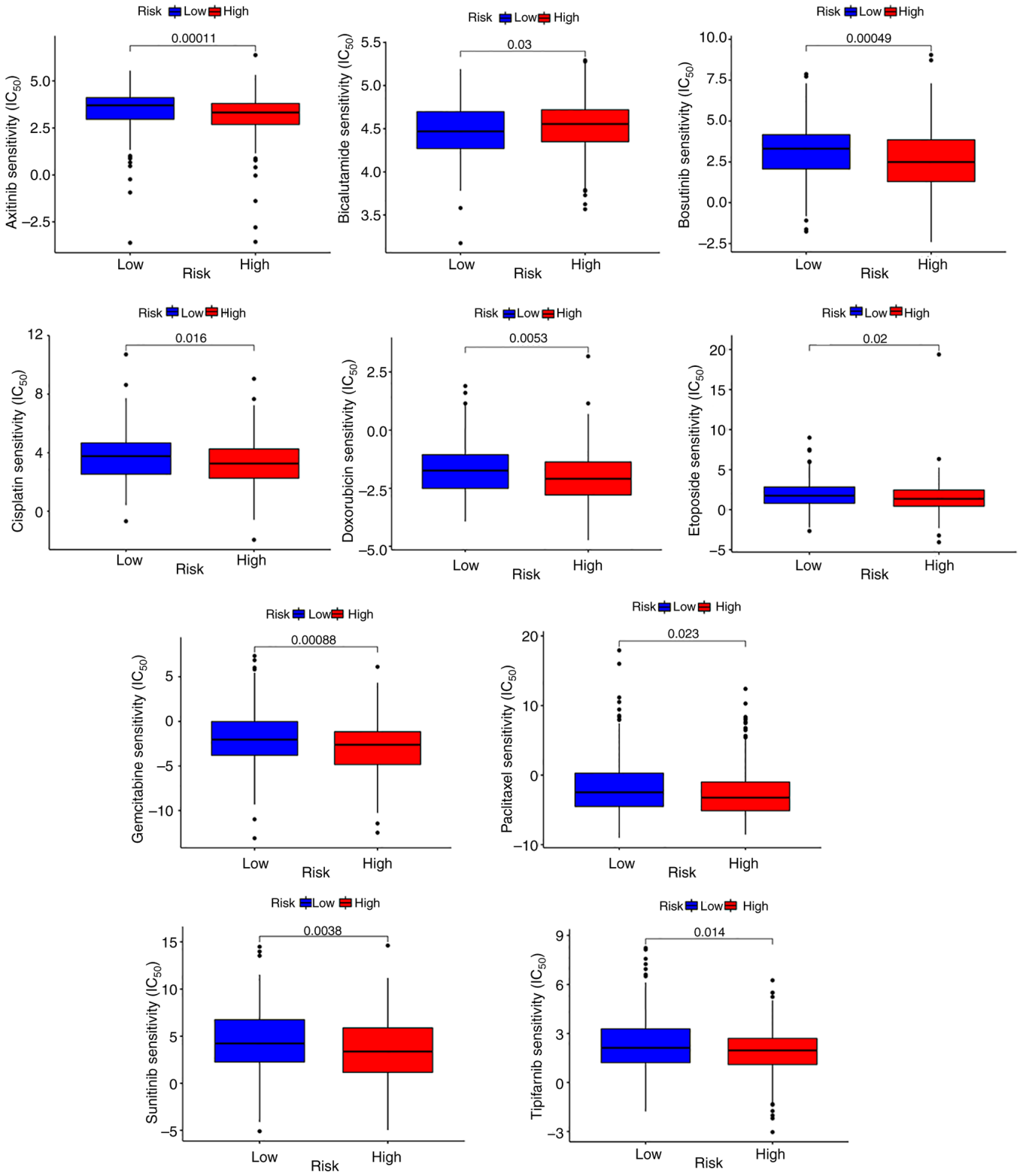

Figure 7. Drug sensitivity analysis. The box plots show the difference in IC_{50} values between high- and low-risk groups for 10 drugs. IC_{50}, half maximal inhibitory concentration.

cuproptosis in the immunological microenvironment of PCa was investigated.

In the present study, patients were randomly divided into a training set and a testing set. Statistical analysis between the two datasets showed no statistical difference in age, pathological T stage, clinical T stage, pathological N stage and Gleason score between the two datasets. This indicates that the two datasets are independent, and the partitioning of datasets is reasonable. The 6-CRL signature effectively categorized patients with PCa into high- and low-risk groups, and the principal component analysis also validated the distinguishing ability of the signature in all three sets.

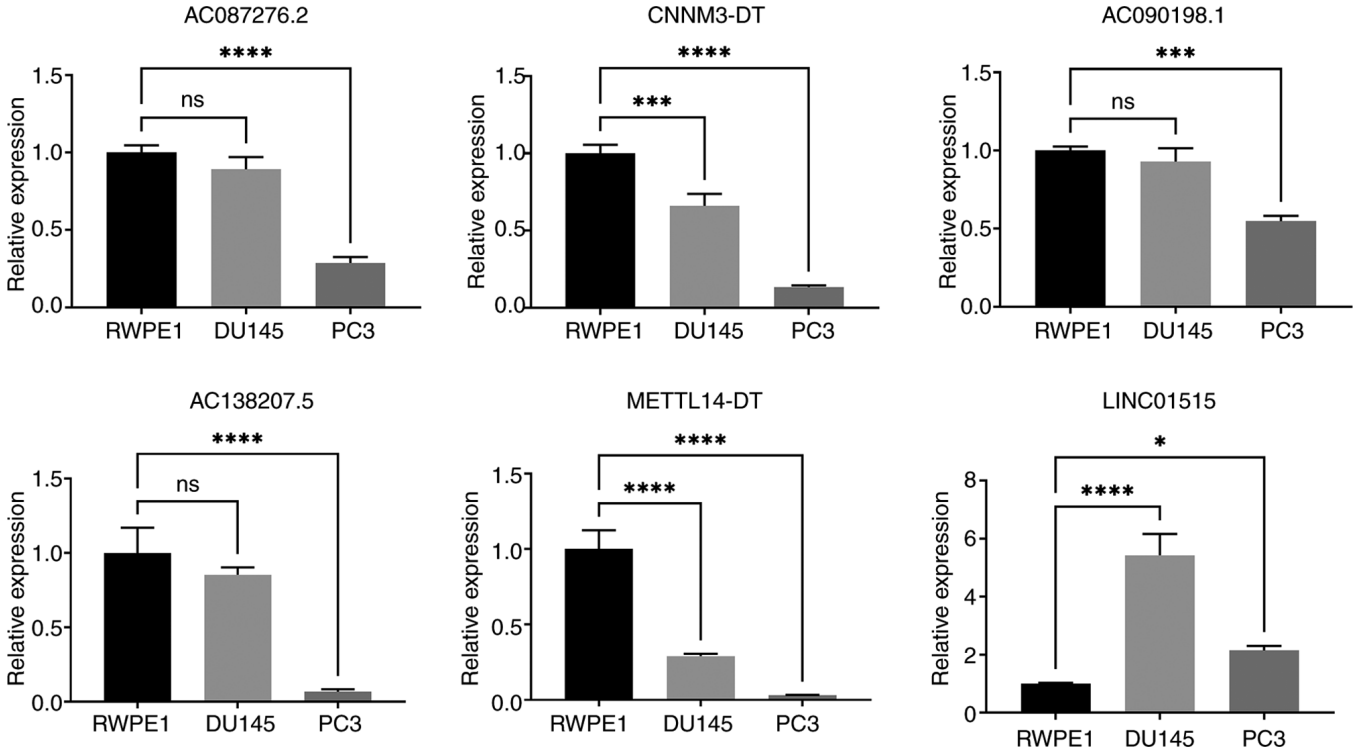

Figure 8. Expression of AC087276.2, CNNM3-DT, AC090198.1, AC138207.5, METTL14-DT and LINC01515 in a normal prostate epithelial cell line (RWPE1) and prostate cancer cell lines (DU145 and PC3), as determined by reverse transcription-quantitative PCR. ns, not significant; *P<0.05, ***P<0.001 ****P<0.0001.

The BFS rate of the high-risk group was significantly lower compared with that in the low-risk group. The predictive accuracy of the signature was estimated and validated through the time-dependent ROC curves in training, testing and entire sets. Notably, the highest AUC value of the signature was in year 5, followed by years 3 and 1. The ROC curves indicated that the signature had a stronger predictive power for BCR of patients with PCa in the long term. In addition, through C-index analysis, it was shown that the C-index value of the signature in the training and entire sets was >0.7, while the relevant value for the testing set was only >0.6. The signature in the testing set was less accurate than that in the training and the entire set; the reason for this difference may be that the sample size of the testing set was small (n=123). The same reason applies to independent prognostic analysis. In the Cox regression analysis, the signature was identified as an independent prognosis factor in both the training set and the entire set, but not in the testing set. The reason for this difference may also be due to the large sample size difference.

By evaluating the accuracy of the six CRLs in each dataset, it was shown that the signature may be a good indicator for predicting BFS in PCa, which was suiTable for both the early and advanced stages. It was also revealed that the signature was related to the PFS of PCa, emphasizing its significance in predicting PCa survival. High-risk patients expressed lower levels of IDO1 than low-risk patients, and these patients had a worse prognosis. Ferreira *et al* (51) reported that patients with PCa who expressed lower levels of IDO1 had a shorter BFS, which is consistent with the findings of the present study that revealed a negative association between IDO1 expression and BCR risk.

In the GO analysis, it was shown that the DEGs between the high- and low-risk groups were mainly enriched in terms associated with the muscle system. In the KEGG analysis, it was demonstrated that the DEGs were involved in steroid hormone biosynthesis. Androgens are steroid hormones that serve an important role in the occurrence and development of PCa. It may be hypothesized that differences in the ability to synthesize androgens contributes to the difference in BCR risk between the two groups. Moreover, the low-risk group had higher TIDE scores. Notably, it has been reported that higher TIDE scores indicate decreased sensitivity to both anti-PD-1 and anti-CTLA-4 treatments (52). The TIDE analysis hypothesized that high-risk patients with PCa may respond better to immunotherapy, and the low-risk population may not be sensitive to immunotherapy. Based on the TIDE score difference, unnecessary immunotherapy may be avoided. The TMB analysis revealed that patients with higher TMB levels had a poor BFS, which was consistent with the findings of a previous study by Luo *et al* (53). In the K-M survival analysis of integrated TMB score and 6-CRL signature, the BFS rate was the lowest for the high-risk group with high-TMB, whereas the highest BFS rate was detected in the low-risk group with high-TMB. Finally, the risk score, Gleason score and pathological T stage were incorporated into a predictive nomogram to predict the 1-, 3- and 5-year BFS rates in patients with PCa. ROC curves, calibration curves and C-index analysis assessed the predictive capability of the nomogram, which has the potential to become a practical tool in clinical decision-making.

In the potential clinical application, this signature could be used to distinguish between BCR high- and low-risk patient with PCa. For high-risk patients, active measures, such as shortening the review time and changing the original treatment regimen, may be taken to reduce the risk of BCR

in this population. In addition, through the nomogram, the probability of BCR in the next 5 years can be calculated, the high-risk population can be identified, and early intervention or enhanced follow-up can be carried out to improve the prognosis of patients. Since this signature only requires the expression of six lncRNAs to calculate the risk score, and does not increase the economic burden on patients, it may have potential clinical application. Furthermore, since only other patient clinicopathological parameters have to be integrated to calculate the probability of BCR through the nomogram, this indicates the simplicity of this signature.

Although Ren *et al* (54) also built a CRL signature to predict the BCR of PCa, the present study differs from this previous study. In the previous study, the CRLs extracted by the author were based on 10 CRGs, whereas the present study was based on 19 CRGs. The number of CRGs included was more extensive and relatively more comprehensive. In addition, only ROC curve analysis was used in the previous study to evaluate the model prediction efficiency. By contrast, principal component analysis was also performed in the present study, providing a more comprehensive evaluation of the model. Moreover, in the previous study, only an overall ROC curve analysis was performed and ROC curve analyses at multiple time points was not carried out, whereas the present study evaluated the prediction efficiency at 1, 3 and 5 years in a more detailed manner. The AUC values in their models were 0.766, 0.613 and 0.693, respectively. The 1-, 3- and 5-year AUC values of the model generated in the present study for the training set were 0.728, 0.740 and 0.783, respectively; those for the testing set were 0.667, 0.715 and 0.831 respectively; and those for the entire set were 0.717, 0.729 and 0.781, respectively. Therefore, the model generated in the present study is probably more accurate than that generated in the previous study. Although the model in the present study was also built based on six lncRNAs, the lncRNAs in the two models were completely different. The RT-qPCR results of the cell lines used in the present study showed that, except for LINC01515, the expression levels of the other five lncRNAs in PCa cells were lower than those in RWPE1 cells. In particular, the expression levels of CNNM3-DT and METTL14-DT in the PC3 and DU145 advanced PCa cells were lower than those in RWPE1 cells. These results suggested that CNNM3-DT and METTL14-DT may play an important role in the progression of advanced PCa.

Notably, the signature assessed in the present study also has certain limitations with regard to its clinical application. First, the construction of this signature was based on patient tumor samples from TCGA, and most of the patients in TCGA dataset are from North America. The applicability of this signature to Asian countries requires further clinical verification. Second, the evaluation of the accuracy of this model was based on retrospective data, and further prospective multicenter clinical studies are required to support its accuracy. In addition, this model was only applicable to patients undergoing radical prostatectomy, but not radical radiotherapy.

The present study also has several limitations. Data from other databases are required for external validation, since just TCGA database was used for internal validation. In addition, although PCa cell lines were used to validate the expression of the signature lncRNAs, the regulatory effect and underlying mechanisms of CRLs in PCa require further biological research.

In the current study, a new signature for predicting BCR based on six lncRNAs was established. Notably, the generated prognostic nomogram containing the 6-CRL signature and other patient clinicopathological characteristics may serve as a clinical tool for decision-making.

Acknowledgements

Not applicable.

Funding

This work was supported by the National Natural Science Foundation of China (grant no. 82260598), the Jiangxi Provincial Academic and Technical Leaders Program (grant no. 20225BCJ22009) and the Research Topic of Traditional Chinese Medicine in Jiangxi Province (grant no. 2018A132).

Availability of data and materials

The transcriptome and clinical data of patients may be found in TCGA (TCGA-PRAD) at the following URL: https://portal.gdc.cancer.gov/. The other data generated in the present study may be requested from the corresponding author.

Authors' contributions

ZJY and TZ designed the study and contributed to the acquisition of TCGA data. ZJY constructed and validated the predictive model, and performed immune analysis. HCC performed TMB analysis and drug sensitivity analysis. ZJY and HHD conducted cell culture and RT-qPCR. HCC and HHD confirm the authenticity of all the raw data. ZJY and HHD drafted the manuscript and drew all figures. ZJY and ZS analyzed and interpreted the data. HCC reviewed and revised the manuscript. HCC reviewed all the figures. TZ contributed to the supervision and administration of the study. All authors read and approved the final version of the manuscript.

Ethics approval and consent to participate

Not applicable.

Patient consent for publication

Not applicable.

Competing interests

The authors declare that they have no competing interests.

References

1. Cronin KA, Scott S, Firth AU, Sung H, Henley SJ, Sherman RL, Siegel RL, Anderson RN, Kohler BA, Benard VB, *et al*: Annual report to the nation on the status of cancer, part 1: National cancer statistics. Cancer 128: 4251-4284, 2022.

2. Siegel RL, Miller KD, Fuchs HE and Jemal A: Cancer statistics, 2021. CA Cancer J Clin 71: 7-33, 2021.
3. Mottet N, van den Bergh RCN, Briers E, Van den Broeck T, Cumberbatch MG, De Santis M, Fanti S, Fossati N, Gandaglia G, Gillessen S, *et al*: EAU-EANM-ESTRO-ESUR-SIOG guidelines on prostate cancer-2020 update. Part 1: Screening, diagnosis, and local treatment with curative intent. Eur Urol 79: 243-262, 2021.
4. Cornford P, van den Bergh RCN, Briers E, Van den Broeck T, Cumberbatch MG, De Santis M, Fanti S, Fossati N, Gandaglia G, Gillessen S, *et al*: EAU-EANM-ESTRO-ESUR-SIOG guidelines on prostate cancer. Part II-2020 update: Treatment of relapsing and metastatic prostate cancer. Eur Urol 79: 263-282, 2021.
5. Liesenfeld L, Kron M, Gschwend JE and Herkommer K: Prognostic factors for biochemical recurrence more than 10 years after radical prostatectomy. J Urol 197: 143-148, 2017.
6. Szerdahelyi P and Kása P: Histochemical demonstration of copper in normal rat brain and spinal cord. Evidence of localization in glial cells. Histochemistry 85: 341-347, 1986.
7. Blockhuys S, Celauro E, Hildesjö C, Feizi A, Stål O, Fierro-González JC and Wittung-Stafshede P: Defining the human copper proteome and analysis of its expression variation in cancers. Metallomics 9: 112-123, 2017.
8. Ge EJ, Bush AI, Casini A, Cobine PA, Cross JR, DeNicola GM, Dou QP, Franz KJ, Gohil VM, Gupta S, *et al*: Connecting copper and cancer: From transition metal signalling to metalloplasia. Nat Rev Cancer 22: 102-113, 2022.
9. Tsvetkov P, Coy S, Petrova B, Dreishpoon M, Verma A, Abdusamad M, Rossen J, Joesch-Cohen L, Humeidi R, Spangler RD, *et al*: Copper induces cell death by targeting lipoylated TCA cycle proteins. Science 375: 1254-1261, 2022.
10. Wang Y, Liu K, Shen K, Xiao J, Zhou X, Cheng Q, Hu L, Fan H, Ni P, Xu Z, *et al*: A novel risk model construction and immune landscape analysis of gastric cancer based on cuproptosis-related long noncoding RNAs. Front Oncol 12: 1015235, 2022.
11. Park A, Lee J, Mun S, Kim DJ, Cha BH, Moon KT, Yoo TK and Kang HG: Identification of transcription factor YY1 as a regulator of a prostate cancer-specific pathway using proteomic analysis. J Cancer 8: 2303-2311, 2017.
12. Ulitsky I: Evolution to the rescue: Using comparative genomics to understand long non-coding RNAs. Nat Rev Genet 17: 601-614, 2016.
13. Tan YT, Lin JF, Li T, Li JJ, Xu RH and Ju HQ: LncRNA-mediated posttranslational modifications and reprogramming of energy metabolism in cancer. Cancer Commun (Lond) 41: 109-120, 2021.
14. Li C, Hu J, Hu X, Zhao C, Mo M, Zu X and Li Y: LncRNA SNHG9 is a prognostic biomarker and correlated with immune infiltrates in prostate cancer. Transl Androl Urol 10: 215-226, 2021.
15. Jiang N, Meng X, Mi H, Chi Y, Li S, Jin Z, Tian H, He J, Shen W, Tian H, *et al*: Circulating lncRNA XLOC_009167 serves as a diagnostic biomarker to predict lung cancer. Clin Chim Acta 486: 26-33, 2018.
16. Chao Y and Zhou D: lncRNA-D16366 is a potential biomarker for diagnosis and prognosis of hepatocellular carcinoma. Med Sci Monit 25: 6581-6586, 2019.
17. Wang Y, Chen W, Lian J, Zhang H, Yu B, Zhang M, Wei F, Wu J, Jiang J, Jia Y, *et al*: The lncRNA PVT1 regulates nasopharyngeal carcinoma cell proliferation via activating the KAT2A acetyltransferase and stabilizing HIF-1α. Cell Death Differ 27: 695-710, 2020.
18. Ghildiyal R, Sawant M, Renganathan A, Mahajan K, Kim EH, Luo J, Dang HX, Maher CA, Feng FY and Mahajan NP: Loss of long noncoding RNA *NXTAR* in prostate cancer augments androgen receptor expression and enzalutamide resistance. Cancer Res 82: 155-168, 2022.
19. Jiang X, Guo S, Xu M, Ma B, Liu R, Xu Y and Zhang Y: TFAP2C-mediated lncRNA PCAT1 inhibits ferroptosis in docetaxel-resistant prostate cancer through c-Myc/miR-25-3p/SLC7A11 signaling. Front Oncol 12: 862015, 2022.
20. Wen S, Wei Y, Zen C, Xiong W, Niu Y and Zhao Y: Long non-coding RNA NEAT1 promotes bone metastasis of prostate cancer through N6-methyladenosine. Mol Cancer 19: 171, 2020.
21. Hung CL, Wang LY, Yu YL, Chen HW, Srivastava S, Petrovics G and Kung HJ: A long noncoding RNA connects c-Myc to tumor metabolism. Proc Natl Acad Sci USA 111: 18697-18702, 2014.
22. Shang Z, Yu J, Sun L, Tian J, Zhu S, Zhang B, Dong Q, Jiang N, Flores-Morales A, Chang C and Niu Y: LncRNA PCAT1 activates AKT and NF-κB signaling in castration-resistant prostate cancer by regulating the PHLPP/FKBP51/IKKα complex. Nucleic Acids Res 47: 4211-4225, 2019.
23. Chade DC, Shariat SF, Cronin AM, Savage CJ, Karnes RJ, Blute ML, Briganti A, Montorsi F, van der Poel HG, Van Poppel H, *et al*: Salvage radical prostatectomy for radiation-recurrent prostate cancer: A multi-institutional collaboration. Eur Urol 60: 205-210, 2011.
24. Molina-Barrera ÁM, Ramos-Ulloa JG, Becerra-Méndez LM, García-Valencia J, Varela-Ramírez R and Silva-Chacón D: Predictors of biochemical recurrence after radical prostatectomy at an oncology reference center in Colombia. Arch Esp Urol 74: 656-663, 2021 (In Spanish).
25. Tilki D, Preisser F, Graefen M, Huland H and Pompe RS: External validation of the European association of urology biochemical recurrence risk groups to predict metastasis and mortality after radical prostatectomy in a European cohort. Eur Urol 75: 896-900, 2019.
26. Mengual L: Molecular technology to optimize the use of biomarkers in the clinic. Arch Esp Urol 75: 103-112, 2022 (In Spanish).
27. Hristova VA and Chan DW: Cancer biomarker discovery and translation: Proteomics and beyond. Expert Rev Proteomics 16: 93-103, 2019.
28. Xie J, Yang Y, Gao Y and He J: Cuproptosis: Mechanisms and links with cancers. Mol Cancer 22: 46, 2023.
29. Goyal B, Yadav SRM, Awasthee N, Gupta S, Kunnumakkara AB and Gupta SC: Diagnostic, prognostic, and therapeutic significance of long non-coding RNA MALAT1 in cancer. Biochim Biophys Acta Rev Cancer 1875: 188502, 2021.
30. Zhang Z, Ma Y, Guo X, Du Y, Zhu Q, Wang X and Duan C: FDX1 can impact the prognosis and mediate the metabolism of lung adenocarcinoma. Front Pharmacol 12: 749134, 2021.
31. Tsvetkov P, Detappe A, Cai K, Keys HR, Brune Z, Ying W, Thiru P, Reidy M, Kugener G, Rossen J, *et al*: Mitochondrial metabolism promotes adaptation to proteotoxic stress. Nat Chem Biol 15: 681-689, 2019.
32. Solmonson A, Faubert B, Gu W, Rao A, Cowdin MA, Menendez-Montes I, Kelekar S, Rogers TJ, Pan C, Guevara G, *et al*: Compartmentalized metabolism supports midgestation mammalian development. Nature 604: 349-353, 2022.
33. Ji L, Zhao G, Zhang P, Huo W, Dong P, Watari H, Jia L, Pfeffer LM, Yue J and Zheng J: Knockout of MTF1 inhibits the epithelial to mesenchymal transition in ovarian cancer cells. J Cancer 9: 4578-4585, 2018.
34. Masisi BK, El Ansari R, Alfarsi L, Rakha EA, Green AR and Craze ML: The role of glutaminase in cancer. Histopathology 76: 498-508, 2020.
35. Luo JP, Wang J and Huang JH: CDKN2A is a prognostic biomarker and correlated with immune infiltrates in hepatocellular carcinoma. Biosci Rep 41: BSR20211103, 2021.
36. Newman AM, Liu CL, Green MR, Gentles AJ, Feng W, Xu Y, Hoang CD, Diehn M and Alizadeh AA: Robust enumeration of cell subsets from tissue expression profiles. Nat Methods 12: 453-457, 2015.
37. Zhang H, Cui B, Zhou Y, Wang X, Wu W, Wang Z, Dai Z, Cheng Q and Yang K: B2M overexpression correlates with malignancy and immune signatures in human gliomas. Sci Rep 11: 5045, 2021.
38. Chen Z, Chen J, Ren D, Zhang J, Yang Y, Zhang H, Mao B and Ma H: EPHA5 mutations predict survival after immunotherapy in lung adenocarcinoma. Aging (Albany NY) 13: 598-618, 2020.
39. Wang G, Xu D, Zhang Z, Li X, Shi J, Sun J, Liu HZ, Li X, Zhou M and Zheng T: The pan-cancer landscape of crosstalk between epithelial-mesenchymal transition and immune evasion relevant to prognosis and immunotherapy response. NPJ Precis Oncol 5: 56, 2021.
40. Jiang P, Gu S, Pan D, Fu J, Sahu A, Hu X, Li Z, Traugh N, Bu X, Li B, *et al*: Signatures of T cell dysfunction and exclusion predict cancer immunotherapy response. Nat Med 24: 1550-1558, 2018.
41. Livak KJ and Schmittgen TD: Analysis of relative gene expression data using real-time quantitative PCR and the 2(-Delta Delta C(T)) method. Methods 25: 402-408, 2001.
42. Tsang T, Posimo JM, Gudiel AA, Cicchini M, Feldser DM and Brady DC: Copper is an essential regulator of the autophagic kinases ULK1/2 to drive lung adenocarcinoma. Nat Cell Biol 22: 412-424, 2020.
43. Shanbhag VC, Gudekar N, Jasmer K, Papageorgiou C, Singh K and Petris MJ: Copper metabolism as a unique vulnerability in cancer. Biochim Biophys Acta Mol Cell Res 1868: 118893, 2021.
44. Denoyer D, Pearson HB, Clatworthy SA, Smith ZM, Francis PS, Llanos RM, Volitakis I, Phillips WA, Meggyesy PM, Masaldan S and Cater MA: Copper as a target for prostate cancer therapeutics: Copper-ionophore pharmacology and altering systemic copper distribution. Oncotarget 7: 37064-37080, 2016.

45. Xie F and Peng F: Reduction in copper uptake and inhibition of prostate cancer cell proliferation by novel steroid-based compounds. Anticancer Res 41: 5953-5958, 2021.
46. Safi R, Nelson ER, Chitneni SK, Franz KJ, George DJ, Zalutsky MR and McDonnell DP: Copper signaling axis as a target for prostate cancer therapeutics. Cancer Res 74: 5819-5831, 2014.
47. Huynh TT, van Dam EM, Sreekumar S, Mpoy C, Blyth BJ, Muntz F, Harris MJ and Rogers BE: Copper-67-labeled bombesin peptide for targeted radionuclide therapy of prostate cancer. Pharmaceuticals (Basel) 15: 728, 2022.
48. Bao JH, Lu WC, Duan H, Ye YQ, Li JB, Liao WT, Li YC and Sun YP: Identification of a novel cuproptosis-related gene signature and integrative analyses in patients with lower-grade gliomas. Front Immunol 13: 933973, 2022.
49. Zhang G, Sun J and Zhang X: A novel cuproptosis-related LncRNA signature to predict prognosis in hepatocellular carcinoma. Sci Rep 12: 11325, 2022.
50. Bian Z, Fan R and Xie L: A novel cuproptosis-related prognostic gene signature and validation of differential expression in clear cell renal cell carcinoma. Genes (Basel) 13: 851, 2022.
51. Ferreira JM, Dellê H, Camacho CP, Almeida RJ, Reis ST, Matos YST, Lima AMR, Leite KRM, Pontes-Júnior J and Srougi M: Indoleamine 2,3-dioxygenase expression in the prognosis of the localized prostate cancer. Int Urol Nephrol 52: 1477-1482, 2020.
52. Woo SR, Corrales L and Gajewski TF: The STING pathway and the T cell-inflamed tumor microenvironment. Trends Immunol 36: 250-256, 2015.
53. Luo C, Chen J and Chen L: Exploration of gene expression profiles and immune microenvironment between high and low tumor mutation burden groups in prostate cancer. Int Immunopharmacol 86: 106709, 2020.
54. Ren L, Yang X, Wang W, Lin H, Huang G, Liu Z, Pan J and Mao X: A cuproptosis-related LncRNA signature: Integrated analysis associated with biochemical recurrence and immune landscape in prostate cancer. Front Genet 14: 1096783, 2023.